Article

Synthesis, Characterization, and Catalytic Performance of a New Heterobimetallic Y/Tb Metal−Organic Framework with High Catalytic Activity

Mireya E. López-Vargas, Juana M. Pérez, Estitxu Echenique-Errandonea, Arantxa Forte-Castro, Sara Rojas, José M. Seco, Antonio Rodríguez-Diéguez, Iñigo J. Vitorica-Yrezabal,* and Ignacio Fernández*

Read Online

ACCESS | Metrics & More | Article Recommendations | Supporting Information

ABSTRACT: A three-dimensional heterobimetallic porous structure with the formula $\{[Y_{3.5}Tb_{1.5}L_6(OH)_3(H_2O)_{1.5}\ (DMF)_{1.5}]_n \cdot 1.5H_2O \cdot DMF\}_n$ (L = 3-amino-4-hydroxybenzoate) (**Y/Tb-MOF**) has been synthesized and characterized by single crystal and powder X-ray diffraction, scanning electron microscopy with energy dispersive X-ray spectroscopy (SEM-EDX), inductively coupled plasma mass spectrometry (ICP-MS), electrophoretic mobility, and Fourier transform infrared (FTIR) spectroscopy. The structure presents two metal environments: a bioaugmented isosceles wedge (mm2) MO_8 and a tricapped trigonal prism (−6m2) MN_3O_6. These configurations facilitate the creation of channels with a diameter of 10.7 Å, enabling its utilization as an active catalyst where the heterobimetallic nature of the assembly will be explored. This mixed-metal metal−organic framework has been tested in the cycloaddition of epoxides with carbon dioxide as well as in the cyanosilylation and hydroboration reactions of carbonylic substrates. Additionally, a monometallic **Tb-MOF** analogue has been synthesized for comparative evaluation of their catalytic performances. Both the mixed metal and monometallic variants exhibit outstanding activity in the cyanosilylation and hydroboration of carbonyls and in the synthesis of carbonates under CO_2 pressure. However, only the latter exhibits high recyclability.

Bimetallic Y/Tb MOF
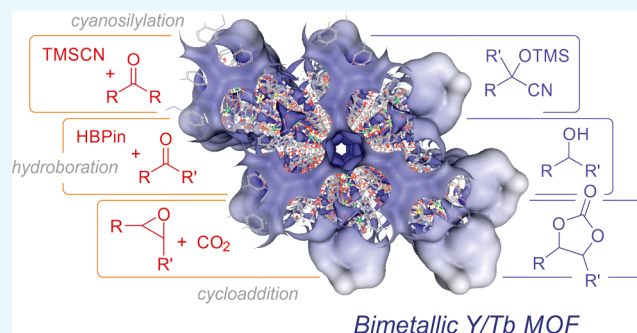
INTRODUCTION

Metal−organic frameworks (MOFs) are hybrid compounds between organic and inorganic materials.[1] They are formed by metal ion nodes linked by multidentate organic ligands forming a three-dimensional assembly that includes porous channels of large superficial area.[2−4] The intrinsic porosity of these MOFs together with their easy tunability and functionalization have made them attractive for multiple applications, especially in heterogeneous catalysis.[5,6] Some examples are the binuclear Ni(II)-based metal−organic framework[7] or those based on polyoxometalate-based Ag−organic compounds that employ 1,3,5-tri(4-carboxylphenyl)-benzene (H_3btb) and 3-(4*H*-1,2,4-triazol-4-yl)benzoic acid (Htba) as ligands, respectively, that were applied in the synthesis of benzimidazoles and pyrazoles.[8] In addition, MOF compounds have garnered significant attention from the scientific community as potential functional materials.[9,10] When a second metal is incorporated into the nodes of the framework, then bimetallic architectures are generated, which could exist as "solid solution" or "core−shell" structures.[11] The partial substitution by this second metal ion in the inorganic nodes ("solid solution") or in a secondary building unit

("core−shell") will allow the bimetallic system to show synergistic effects, even enhanced properties compared to their monometallic counterparts, exhibiting superior performance in many applications, including catalysis.[12,13] These bimetallic systems can be synthesized by direct synthesis, postsynthetic modification, and template synthesis, although it should be convenient to use metals having the same Coulumbic charge and ionic radius in order to increase the chances of having simultaneous and homogeneous co-incorporation of the two metals. In addition, the limitations of current characterization techniques in terms of addressing the distribution of various metals and the possibility of the preferential location of these metals at the core or over the external surface as a consequence of the preparation procedure are still not solved.
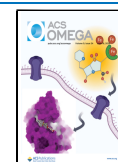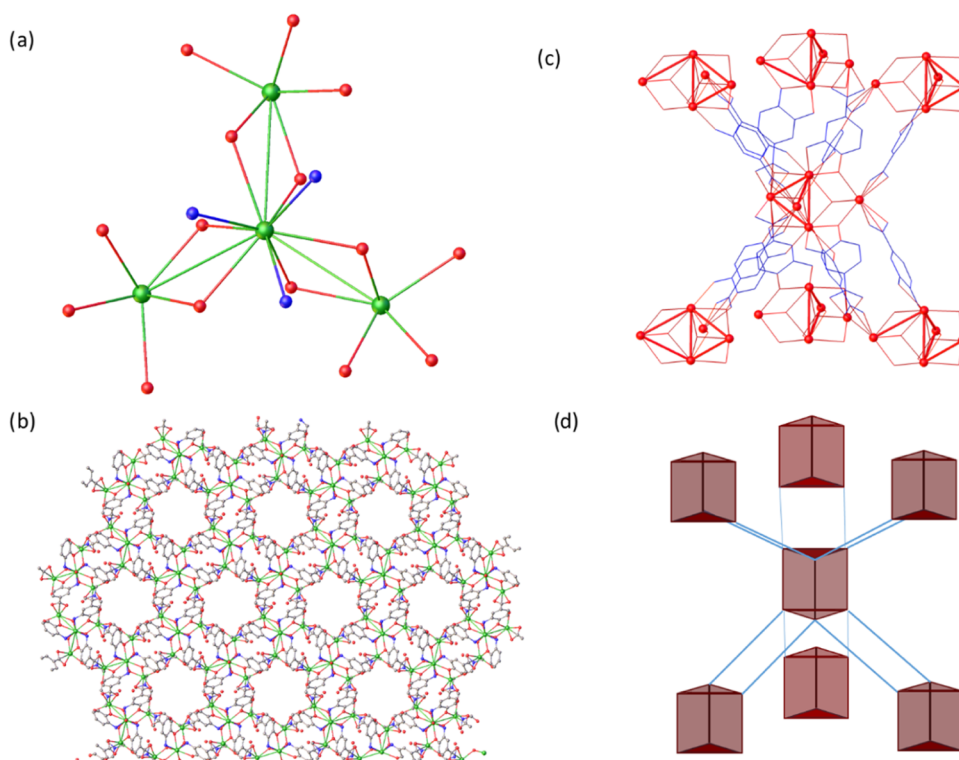
Figure 1. (a) Top view of the $M_5N_6O_{30}$ core of the **Y/Tb-MOF** SBU; carbons and hydrogens are removed for clarity. (b) (001) view of the **Y/Tb-MOF** structure showing the pores across the (001) direction. Color code: Y/Tb atoms in green, oxygen in red, nitrogen in blue, and carbon in gray. (c) Acs topological network with the $(4^9 \cdot 6^6)$ of **Y/Tb-MOF**. (d) Scheme of the acs $(4^9 \cdot 6^6)$ topological network where each $M_5N_6O_{30}$ metal core is connected to six others by two 3-amino-4-hydroxybenzoate ligands. Red trigonal prism and metal clusters were represented in red, and 3-amino-4-hydroxybenzoate ligands were represented in blue.

Stable rare-earth (RE) metal−organic frameworks (RE-MOFs) are considered promising materials for gas storage, separation, and processing, where the presence of multiple Lewis acidic/basic sites allows the catalytic transformation of some of these gases such as CO_2.[10] The cycloaddition reaction of CO_2 to an epoxide under mild conditions is attractive industrially, as the resulting carbonate product is a useful chemical for industrial applications.[14] A relatively large set of terbium MOFs, and to a lesser extent those based on yttrium, have been used in the cycloaddition reactions of CO_2 (Table S12). Among them, the ones described by Chen et al. (NUC-53)[15] and Wei et al. (RE-BDC and RE-NDC)[16] stand out with conversions from good to excellent with TOF values of 495 h^{-1} for NUC-53 and in the range of 400−509 h^{-1} for those developed by Wei et al.[16] In addition, these systems could be recycled up to five times, proving to be suitable heterogeneous catalysts for the cycloaddition of CO_2 with epoxides.

The formation of C−C bonds by the addition of trimethylsilyl cyanide (TMSCN) to carbonyl compounds to form cyanohydrin trimethylsilyl ethers is another reaction of interest. The products of this reaction can be transformed into a wide range of new products or synthetic intermediates such as α-hydroxy acids, α-hydroxyaldehydes, and β-aminoalcohols.[17−20] This reaction has been studied using MOF catalysts based on Cu, Cr, Mn, Fe, Co, and Zr, among others,[21] including RE-MOFs (Table S13).[17−43] Interestingly, most of these works focus on aldehydes as the most reactive substrates, with only few examples focused on the less reactive ketones.[44] These endeavors, however, yield new quaternary centers of great interest from the point of view of asymmetric organic synthesis.[21,40] A remarkable Y-MOF catalyst was developed by

Echenique-Errandonea et al.,[34] which yields full conversion of benzaldehyde to the desired product in 5 h with a 0.5 mol % catalyst. Furthermore, it could be recycled seven times without loss of catalytic activity, having a TOF value of 106 h^{-1}, which is considerably higher than other catalysts reported (Tb-TCA,[17] Y/Eu-MOF,[35] GR-MOF-12,[36] and Y-DDQ)[32] and similar to Sm/Eu/Gd/Tb/Eu−Gd/Eu−Tb−PSA (PSA = 2-phenylsuccinate)[17] and GR-MOF-6.[18]

Hydroboration reactions have also attracted the attention of the scientific community using MOFs as Lewis acid catalysts.[45] The addition of boranes (HBR_2) to carbonyl bonds leads to the formation of B−O bonds, which, together with hydrolysis, constitutes a two-step process equivalent to a reduction.[46] In this way, derivatized alcohols could be obtained, allowing the synthesis of fine chemicals and natural products.[47] The only studies of RE-MOFs used in hydroboration reactions of carbonyl compounds are those based on Y/Eu-MOF (ligand = 3-amino-4-hydroxybenzoic acid)[34] and GR-MOF-12 (ligand = 2,2′-bicinchoninic acid).[35] Both systems afford the corresponding alcohols with TOF values from 20 to 21 h^{-1} and 3 and 7 cycles of recyclability, respectively (Table S14). The activity of the heterobimetallic Y/Eu-MOF,[35] which shares the same ligand as the Tb and Y/Tb-MOFs described herein, will also be compared.

Within this context, a new three-dimensional heterobimetallic porous structure with the formula $\{[Y_{3.5}Tb_{1.5}L_6(OH)_3(H_2O)_{1.5}(DMF)_{1.5}]_n \cdot 1.5H_2O \cdot DMF\}_n$ (L = 3-amino-4-hydroxybenzoate) (**Y/Tb-MOF**) and its monometallic **Tb-MOF** analogue have been synthesized, characterized, and employed as catalysts in the CO_2 cycloaddition of epoxides and in the cyanosilylation and hydroboration of

carbonylic substrates. These novel systems represent an extension of our work on isostructural metal−organic frameworks based on Y,[34] Eu,[21] Y/Eu,[35] and Dy,[44] with the target of exploring how partial substitution by a second metal will enable the bimetallic system to exhibit synergistic catalytic effects.

■ RESULTS AND DISCUSSION

Synthesis and Characterization of Catalysts. The solvothermal reaction between 3-amino-4-hydroxybenzoate and a 1:2 molar mixture of $Y(NO_3)_3 \cdot 6H_2O$ and $Tb(NO_3)_3 \cdot 5H_2O$ yields a heterobimetallic 3D porous framework that crystallizes in the $P6_3/m$ hexagonal space group. Two metal environments are presented in structures MO_8 and MN_3O_6, which according to continuous shape measurements[48] have been demonstrated to be best fitted with a bioaugmented isosceles wedge (mm2) and a tricapped trigonal prism (−6m2) polyhedral, respectively (Tables S5 and S6).

A MO_8 metallic center is formed by the coordination of two chelating carboxylates, two bridging μ_2-phenoxy, a bridging μ_3-hydroxy, and a disordered DMF/water (50/50) solvent molecule. The MN_3O_6 metallic coordination environment is constituted of three coordinated amino and three bridging μ_2-phenoxy groups from the 3-amino-4-hydroxybenzoate ligand and three bridging μ_3-hydroxy atoms. The secondary building unit is formed by three M_3OH triangles, which share a common M−M edge, forming an $M_5(OH)_3$ core (Figure 1a). Each secondary building unit (SBU) is connected to six other SBUs by two rigid 3-amino-4-hydroxybenzoate ligands, forming a robust acs topological network with the $(4^9 \cdot 6^6)$ point symbol (Figure 1b). The porosity of the structure has been characterized by PLATON-v1.18,[49] exhibiting three different micropores of 480, 108, and 108 $Å^3$, which is in accordance with 19% of the volume of the structure. The channel diameter is 10.7 Å (Figure S1), enabling solvent crystallization molecules to be trapped, and concretely, the electron count obtained from squeeze software in Platon agrees with the presence of a DMF molecule and a water molecule per unit cell in large pores, while 1.5 water molecules were located in small pockets. The refinement of the Y/Tb composition in one of the crystals shows the presence of Y and Tb cations with a 3.55(Y)/1.46(Tb) proportion in each of the two metal types (MO_8 and MN_3O_6) of the asymmetric unit. The fact of using two metals of the same charge and similar radii for yttrium (coordination number 8:1.019 Å; coordination number 9:1.075 Å) and terbium (coordination number 8:1.040 Å; coordination number 9:1.095 Å)[50] allows the simultaneous and homogeneous co-incorporation of the two metals, instead of having one metal in nodal positions preferentially, while the other is present as defects in some amorphous parts of the solid or in an independent solid phase without sharing the crystalline MOF structure.

Interestingly, the metal ratio was constant with no apparent dependence on the ratio of metallic precursors used in the synthesis (1:2, 1:1, and 2:1 for Y/Tb, respectively), yielding, in all of the cases, similar isolated yields of no more than 4 mg. The scaled-up procedure, outlined in the Supporting Information, resulted in higher isolated amounts of 75−85 mg. The purity of all of these compounds was confirmed by powder X-ray diffraction (PXRD).

A comparison among the Dy-,[44] Y-,[34] Eu-,[21] Y/Eu-,[35] and Y/Tb-MOF crystal structures shows cell volume contraction values of 7.5 and 1.2% for Y- and Dy-MOFs, respectively, and

an increase of 3.7, 2.3, and 2.7% for Eu-, Y/Eu-, and Y/Tb-MOFs, respectively. Unit cell a and b axes from Y-MOF present a reduction of 1 Å compared to the lanthanide or mixed metal MOFs while presenting an average increase of 0.6 Å in the c axis. The shorter a and b axes and larger c axis are the result of shorter Y−N (2.497(5) Å) bonds compared with the Eu−N (2.547(3) Å) bonds, which induces a 6.41(1)° angle change between M_5 (M = Eu, Y) clusters (Table S4). The monometallic Dy-MOF falls structurally between the Eu- and Y-MOFs, with intermediate axis lengths of 15.4579 and 17.0864 Å and Dy−N distances of 2.509(7) Å, alongside an average Dy−O distance of 2.405(5) Å (Table S4).

The new MOF system was used for thermogravimetric analysis (TGA and DTG) to investigate its thermal stability between ambient temperature and ca. 1000 °C. The graphs presented in Figure S12 highlight the similarity in patterns with their isostructural counterparts of Dy,[44] Y,[34] and Eu.[21] These patterns reveal three main regions: (i) a weight loss centered at 72 °C, spanning from room temperature up to 177 °C, associated with the gradual loss of solvent molecules (including lattice water molecules and coordinated DMF molecules); (ii) a sudden weight loss between 252 and 438 °C, likely attributed to the collapse of the crystal structure, indicating that solvent molecules play a stabilizing role and their removal promotes crystal structure decomposition; and (iii) a final region with at least three weight losses occurring at 521, 712, and 941 °C, indicative of the decomposition of the organic linkers.

As mentioned previously, all of the isostructural lattices of **Y/Tb-MOF**, whether monometallic based on Dy, Y, or Eu or bimetallic based on Y/Eu, exhibit almost identical assemblies, with only marginal deviations in the case of the yttrium MOF. In this context, the gas adsorption study conducted on the Dy-based MOF[44] was particularly relevant, assuming similar behavior across all structures. It was demonstrated that at the highest pressure of 8 bar, this MOF exhibits relatively low affinity toward N_2 gas, with an adsorption uptake of 1.10 mmol/g, considerably lower than that observed for CO_2, which were 4.59 and 3.84 mmol/g at 273 and 298 K, respectively. Interestingly, the adsorption occurred in two distinct steps at nearly the same loading, irrespective of the adsorption temperature. Such behavior could be attributed to the reorganization of CO_2 at a critical loading to create space for subsequent adsorbate molecules. These findings prompted us to evaluate our MOFs in catalytic cycloaddition reactions involving CO_2, as described below.

Electrophoretic mobility measurements are a useful tool for studying the properties of MOFs in solution. One particular advantage of these types of measurements is their ability to provide information about the surface charge. MOFs often have a high surface area and a large number of charged groups on their surface, which are responsible for their interactions with other molecules or materials. The magnitude of the electrostatic repulsion or attraction between particles is measured by the ζ-potential. These measurements are often used to determine the stability of colloidal dispersions, where particles are suspended in a liquid medium. When the ζ-potential of the particles in the dispersion is relatively large (either positive or negative), they tend to repel each other and remain dispersed, resulting in a stable colloidal suspension. However, if the ζ-potential is small or zero, the particles tend to aggregate and form larger entities, which can lead to instability and the settlement of the suspension. In this study, the measurements were always made at a fixed conductivity of

330 μS/cm, which is equivalent to a concentration of about 2.4 mM NaCl (Figure S20). With both catalysts Y/Tb-MOF and Tb-MOF, the highest negative value of the ζ-potential was reached at pH 11 (-22.4 ± 0.8 and -33.9 ± 1.1 mV for Y/Tb-MOF and Tb-MOF, respectively), suggesting that dissociation of the carboxylate groups has occurred conferring an overall negative charge (Figure 2 and Table S8). When the pH of the
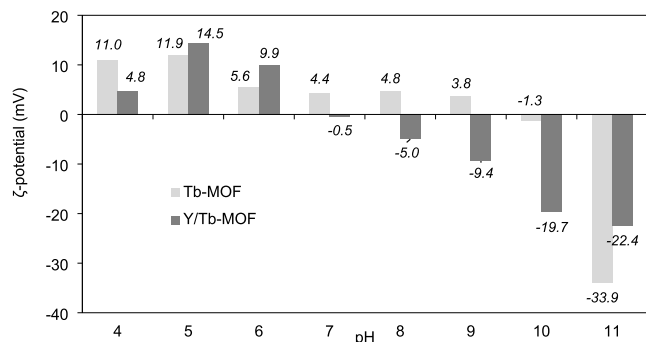

Figure 2. ζ-Potential values obtained as a function of pH for catalysts Y/Tb-MOF and Tb-MOF. All of the measurements were performed with a constant conductivity of 330 μS/cm.

solutions decreases, the ζ-potential values for both assemblies start to increase, evidencing an isoelectric point at ca. 7 in the case of heterobimetallic Y/Tb-MOF and about pH 9 in the case of Tb-MOF. This differential behavior as a function of pH might arise from the different solvation and coordination properties of terbium compared to yttrium, as the presence of the former is key in the increased stability at low pH. Figure 2 illustrates the pH versus ζ-potential graph in the range between 4 and 11 for both catalysts.

Particle size distribution in the suspended and deposited fraction was determined for both catalysts using optical microscopy (Figures S13 and S16). The catalysts were suspended in distilled water (2.5 mg of each MOF in 5 mL of distilled water), and after vigorous stirring, the samples were

left for sedimentation for 5 min, followed by the isolation of the suspended fraction. Then, a sample was taken with a pipet, deposited on a glass slide, and covered with a coverslip. Optical images were recorded showing an average particle size distribution for the deposited fraction of 17 ± 7 μm for Y/Tb-MOF and 15 ± 6 μm for Tb-MOF after the statistical treatment of the images using the ImageJ photographic analysis program (Figure S18). Regarding the suspended fractions, the average size for Y/Tb-MOF was determined to be 9 ± 4 μm, whereas for Tb-MOF, the average size was 11 ± 4 μm (Figure S19).

Single-crystal X-ray diffraction allowed for the proposal of an approximated formula of the heterobimetallic catalyst of $C_{46.5}H_{44.33}N_{7.5}O_{27.5}Tb_{1.46}Y_{3.55}$, which was further confirmed by ICP-MS and SEM-EDX. ICP-MS exhibited yttrium and terbium contents of 149.08 ± 0.75 and 125.83 ± 0.43 g/kg, respectively, which corresponded to a Y/Tb molar ratio of 3.55/1.677, which is in excellent agreement with the ratio of 3.5/1.5 found in the X-ray structure.

Field emission scanning electron microscopy (FESEM) images, employing a backscattered electron detector, revealed the irregular morphology of the synthesized Y/Tb-MOF (Figure 3a,b).

The size distribution range is 40 ± 14 nm, as depicted in the histogram shown in Figure S11. These findings align with the optical images captured for both the deposited and suspended fractions of the MOF. Elemental mapping images confirmed the specified composition, showcasing a uniform distribution of Tb and Y elements across the various particles (Figure 3c,d).

The FTIR spectrum of compound Y/Tb-MOF showed typical bands associated with the organic ligand (Figure S13). A broad band is displayed in the 3191 cm^{-1} region associated with NH and OH bands. In addition, four main peaks in 1656, 1597, 1508, and 1428 cm^{-1} regions are also visible and assigned to the asymmetric stretching vibrations of the carboxylate groups and the aromatic C−C and C−N bonds. The group of signals in the lower range, 1392 and 1283 cm^{-1}, can be linked to symmetric stretching vibrations of the
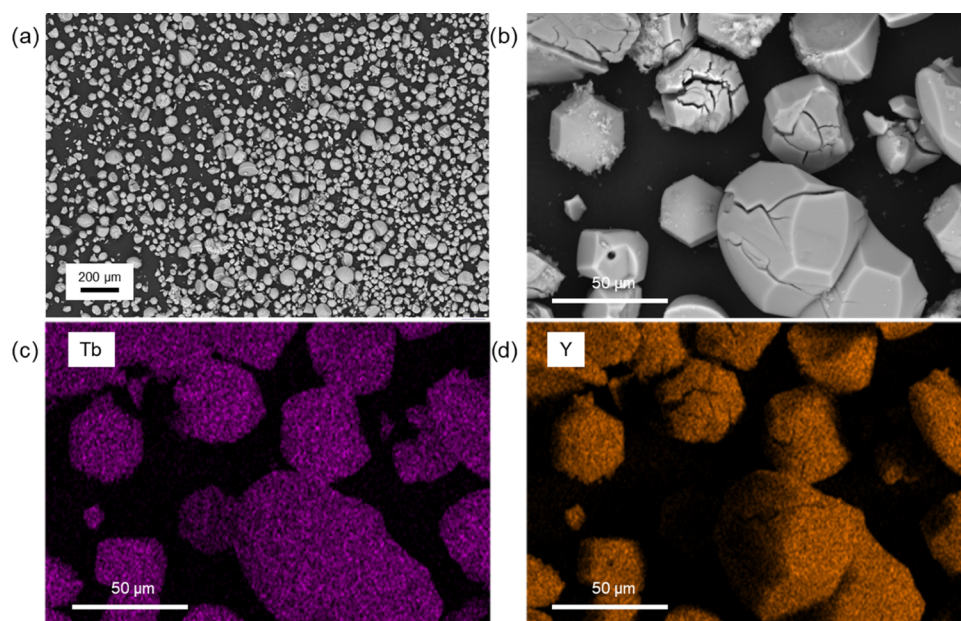

Figure 3. (a, b) FESEM backscattered electrons pictures and (c, d) elemental mapping images of the Y/Tb-MOF catalyst.

Table 1. Scope of the Cyanosilylation Reaction Using Y/Tb-MOF and Tb-MOF[a]

entry	R	R′	product	conversion (%) Y/Tb-MOF	conversion (%) Tb-MOF
1	Ph	Me	**2a**	>99	>99[b]
2	p-MeO−C_6H_4	Me	**2b**	88	(61)[b] 88
3	p-Cl−C_6H_4	Me	**2c**	86	84[b]
4	2-pyridine	Me	**2d**	94	91[b]
5	Et	Me	**2e**	>99	80[b]
6	PhCH=CH	Ph	**2f**	>99	(74)[b,c] >99[c]

[a]Reaction carried out using ketones **1** (0.25 mmol) and TMSCN (34 μL, 0.275 mmol, 1.1 equiv) with 0.5 mol % of the corresponding catalyst under an inert N_2 atmosphere at room temperature obtaining the desired cyanohydrin product **2** after 24 h of reaction. [b]Conversion after 4 h of reaction. [c]Only the 1,2-addition product (**2f**) after the analysis of the reaction crude by ^{1}H NMR spectroscopy.

carboxylate groups. Interestingly, two strong bands at 787 and 658 cm^{-1} assigned to out-of-plane C−H bending observed in trisubstituted aromatic rings, together with some others below 660 cm^{-1}, i.e., 658, 610, 576, 529, and 475 cm^{-1}, which are assigned to the presence of M−O and M−N moieties. Figure S9 shows the FTIR spectrum of **Y/Tb-MOF**, together with its comparison with the free ligand.

Catalytic Activity. The catalytic activity of our new heterobimetallic **Y/Tb-MOF** (0.5 mol %) and monometallic **Tb-MOF** (0.5 mol %) was first evaluated in the cyanosilylation of different ketones (**1**) using TMSCN as a nucleophile, solvent-free reaction conditions, and room temperature under a N_2 atmosphere. These conditions were used previously for the reported monometallic **Y**- or **Eu-MOF**,[19,21] bimetallic **Y/Eu-MOF**,[35] and with catalyst **GR-MOF-6**.[19]

First, the evaluation of the blank reaction using acetophenone (**1a**) was carried out, obtaining no product **2a** after a reaction time of 24 h, whereas in the presence of the catalysts, quantitative conversions were achieved (entry 1, Table 1) after 24 h. To evaluate the scope of the reaction, ketones with different chemical natures such as aromatic with electron-donating groups (**1b**) and electron-withdrawing groups (**1c**), heteroaromatic (**1d**), and also bearing aliphatic substituents (**1e**) were tested (entries 2−5). As can be observed in Table 1, independent of the nature of the substituent, conversions in the 86−99% range were obtained after 24 h of reaction using **Y/Tb-MOF** as a catalyst. Similar conversions were obtained for **Tb-MOF** (80−99%) after only 4 h of reaction. Furthermore, the chemoselectivity of the reaction was tested employing α,β-unsaturated ketone **1f** (entry 6), obtaining full conversion to the desired 1,2-addition product (**2f**) after 24 h of reaction with both catalysts. No traces of the 1,4-addition product were found after inspection of the corresponding ^{1}H NMR spectra of the reaction crudes (Figures S23 and S24). To gain valuable insights into potential catalytic sites involved in the reaction, the starting materials of **Y/Tb-MOF** were utilized as homogeneous catalysts. Y(NO$_3$)$_3$, Tb(NO$_3$)$_3$, and the free ligand were added separately in catalytic runs with the same mol % as the MOF catalyst. Conversions of 91, 89, and 5%, respectively, were achieved, indicating that both yttrium and terbium metals catalyze the reaction, functioning as real active sites in the heterogeneous process.

The kinetic profiles using acetophenone (**1a**) as the model substrate and both catalysts are shown in Figure 4a.

In the case of the heterobimetallic **Y/Tb-MOF** catalyst, an induction period of 152 min is required. The reaction is significantly faster for the **Tb-MOF** catalyst with an induction
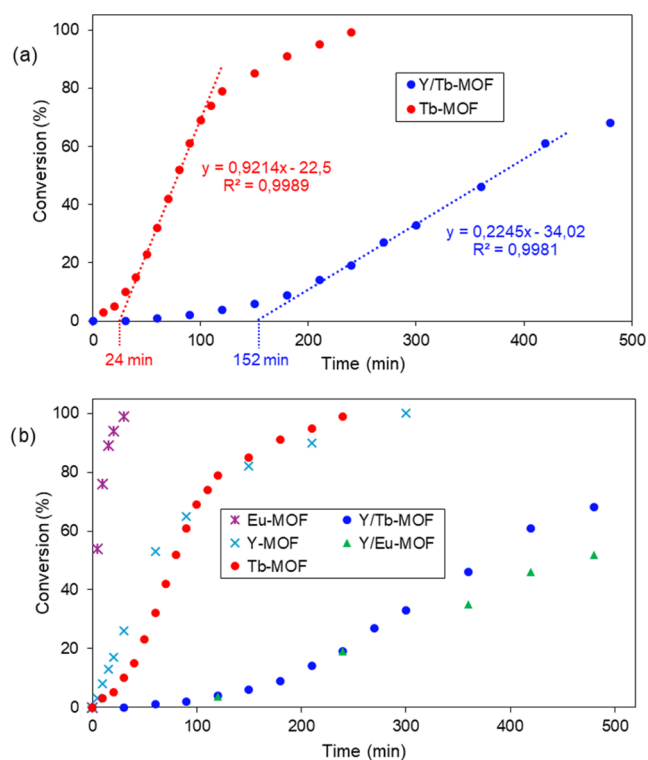

Figure 4. (a) Kinetic profiles for both catalysts in the cyanosilylation reaction of acetophenone (**1a**) using a 0.5 mol % catalyst at room temperature with no solvent. (b) Comparison with MOFs sharing the same ligand (3-amino-4-hydroxybenzoic acid) but with a different metal composition, all under the same catalytic conditions.

period of only 24 min, requiring only 240 min for completion, whereas the **Y/Tb-MOF** catalyst has only a 19% conversion at the same time point. This different initial behavior could be due to several hypotheses: (i) varying leaching rates, (ii) distinct rates of solvent exchange by reactants within the MOF channels, or (iii) a combination of both factors. Interestingly, when comparing the kinetic profiles of **Tb** and **Y/Tb-MOF** with their isostructural monometallic MOFs based on europium[21] and yttrium,[34] as well as with the bimetallic MOF composed of yttrium and europium[35] (Figure 4b), it is evident that the catalytic performance diminishes when mixed-metal MOFs are involved. The bimetallic systems significantly reduce the initial rate, as well as the time to complete full conversion, once again highlighting an antagonistic effect when

Table 2. Scope of the Hydroboration Reaction Using Y/Tb-MOF and Tb-MOF[a]

entry	R	R′	product	conversion (%) Y/Tb-MOF	conversion (%) Tb-MOF
1	Ph	Me	**3a**	91	70
2	p-MeO−C_6H_4	Me	**3b**	90	75
3	p-Cl−C_6H_4	Me	**3c**	85	75
4	2-pyridine	Me	**3d**	60	89
5	Et	Me	**3e**	86	81
6	PhCH=CH	Ph	**3f/3f′**	97 (76/21)[b]	93 (74/19)[b]

[a]Reaction carried out using ketones **1** (0.25 mmol) and HBpin (40 μL, 0.275 mmol, 1.1 equiv) with 0.5 mol % of the corresponding catalyst under an inert N_2 atmosphere at room temperature obtaining the desired secondary alcohol product **3** after 24 h of reaction. [b]Ratio between 1,2- and 1,4-addition products (**3f/3f′**) after the analysis of the reaction crudes by ^{1}H NMR spectroscopy.

monometallic MOFs of terbium or europium are diluted with yttrium.

The turnover frequency (TOF) was also calculated over the course of the reaction as millimoles of product per millimoles of catalyst per unit time (Figures S30 and S31), obtaining a maximum TOF of 17 h^{-1} (61% conversion) for catalyst **Y/Tb-MOF** after 7 h of reaction and a maximum TOF of 83 h^{-1} for catalyst **Tb-MOF** after only 100 min of reaction (69% conversion). This parameter was also calculated for all of the substrates tested in Table 1 reaching similar values (Figures S32 and S33).

Reports of the catalytic role of MOFs in the hydroboration reaction are scarce, with a recent report describing the heterobimetallic **Y/Eu-MOF** catalyst being the only example published.[35] In this reaction, pinacolborane (HBpin) was chosen as a reagent, and the reaction was conducted without a solvent and under a N_2 atmosphere at room temperature. The blank reaction was assayed using acetophenone (**1a**), showing no product after 24 h of reaction time. Then, the scope of the reaction was studied with a variety of ketones, obtaining conversions ranging from 60 to 91% with **Y/Tb-MOF** and from 70 to 89% with **Tb-MOF** (Table 2).

For α,β-unsaturated ketone **1f** (entry 6, Table 2), a mixture of 1,2- and 1,4-addition products was observed in the ^{1}H NMR reaction crudes (Figures S24 and S25). In general, the **Y/Tb-MOF** system provided better conversions than **Tb-MOF** with the exception of heteroaromatic ketone **1d**, where **Tb-MOF** showed 89% conversion compared to the modest 60% afforded by **Y/Tb-MOF**. The values of TON and TOF were also calculated for the hydroboration catalysis when using both catalysts (Figures S34 and S35), obtaining similar values (from 1.4 to 7.6 h^{-1} with **Y/Tb-MOF**, and from 4.2 to 7.4 h^{-1} with **Tb-MOF**) to the previously reported heterobimetallic **Y/Eu-MOF** catalyst.[35] To finish with the study of catalytic activity, we decided to test the formation of cyclic carbonates in the cycloaddition of epoxides and CO_2. This study started with optimization of the reaction conditions (Table 3). The reaction was tested using tetrabutylammonium bromide (TBAB) as a cocatalyst, a temperature of 60 °C, a CO_2 pressure of 5 bar, and a reaction time of 19 h without the use of any solvent. These conditions selected were the same as those reported previously by Zhao et al., except for the increase of CO_2 pressure from 1 to 5 bar and the reaction time of 19 h except for 12 h.[51] The reaction in the absence of any catalyst and cocatalyst was also run (entry 1, Table 3), showing the lack of formation of products. Then, the reaction was performed using only TBAB (2.5 mol %, entry 2, Table 3),

Table 3. Optimization of the Experimental Conditions for the MOF-Catalyzed Reaction of Styrene Oxide (4a) and Carbon Dioxide toward 4-Phenyl-1,3-dioxolan-2-one (5a)[a]

entry	catalyst	cocatalyst	solvent	T (°C)	conv. (%)
1				60	0
2		TBAB		60	11
3	**Y/Tb-MOF**			60	0
4	**Y/Tb-MOF**	TBAB		60	39 (51)[b]
5	**Y/Tb-MOF**	TBAB	DCM	60	2
6	**Y/Tb-MOF**	TBAB	PhMe	60	7
7	**Y/Tb-MOF**	TBAB	DMF	60	6
8	**Y/Tb-MOF**	TBAB	MeOH	60	2
9	**Y/Tb-MOF**	TBAB	ChCl/urea (1:2)	60	34
10[c]	**Y/Tb-MOF**	TBAB		60	37
11	**Y/Tb-MOF**	TBAB		RT	4
12	**Y/Tb-MOF**	TBAB		70	41
13	**Y/Tb-MOF**	TBAB		100	60
14				100	0
15		TBAB		100	24
16	**Tb-MOF**	TBAB		100	58
17	**Tb-MOF**	NaI		100	11
18	**Tb-MOF**	KBr		100	0
19	**Tb-MOF**	ChCl		100	0
20	**Tb-MOF**	$C_{14}H_{42}NBr$		100	0
21	**Tb-MOF**	TBAF		100	0
22	**Tb-MOF**	TBAI		100	49

[a]Reaction carried out using epoxide **4a** (57 μL, 0.5 mmol), obtaining product **5a** after 19 h of reaction using a 2 mol % MOF catalyst. [b]Conversion obtained after 3 days of reaction. [c]Reaction carried out using 6 bar of CO_2.

obtaining 11% conversion to the desired product after 19 h of reaction time. No reaction was observed in the presence of the catalyst and the absence of the cocatalyst (entry 3), thus pointing out the important role of the cocatalyst in this reaction. When the catalyst and cocatalyst were present in the reaction mixture (entry 4), the conversion to **5a** increased up to 39 and 51% after 3 days, respectively. The influence of the solvent in the reaction was also studied by using dichloromethane, toluene, dimethylformamide, and methanol (entries 5−8), obtaining very low conversions in all of the cases. The

Table 4. Scope of the MOF-Catalyzed Cycloaddition Reaction between Three Different Epoxides and Carbon Dioxide[a]

Entry	Substrate	Product	Catalyst	Conversion (%)
1		**5b**	**Y/Tb-MOF**	65
2			**Tb-MOF**	87
3		**5c**	**Y/Tb-MOF**	41
4			**Tb-MOF**	46
5		**5d**	**Y/Tb-MOF**	0
6			**Tb-MOF**	0

[a]Reaction carried out using epoxide **4** (0.5 mmol), obtaining product **5** after 19 h of reaction.

deep eutectic solvent formed by choline chloride and urea in a 1:2 ratio (entry 9) showed conversions similar to those obtained in the absence of the solvent. Surprisingly, the CO_2 pressure increase to 6 bar did not improve the conversions (entry 10). Then, the influence of temperature was assessed using RT, 70, and 100 °C, showing a maximum conversion of 60% at 100 °C (entry 13). The influence of TBAB without the presence of MOF (entry 15) was also studied at 100 °C, obtaining 24% conversion. Under these conditions of temperature, the presence of **Tb-MOF** increased the yield up to 58% (entry 16). The use of different cocatalysts was also explored by using NaI (entry 17), KBr (entry 18), choline chloride (ChCl, entry 19), hexadecyltrimethylammonium bromide ($C_{14}H_{42}NBr$), tetrabutylammonium fluoride (TBAF), and tetrabutylammonium iodide (TBAI, entries 20−22), obtaining reduced conversions and highlighting the relevance of TBAB in this reaction.

Finally, the scope of the reaction was evaluated with both catalysts using three different epoxides (Table 4). The results showed moderate conversions in the cycloaddition of aliphatic 2-butylepoxide (**4b**) and cyclohexane oxide (**4c**), and no conversion when the limonene (**4d**) derivative was employed.

Recyclability and Leaching Studies. The recyclability tests are key to establishing the practical use of the catalysts. After completion of the cyanosilylation reaction with **1a** as a substrate (under optimal reaction conditions), the catalysts were isolated from the reaction mixture via centrifugation and washed with Et_2O. Then, the catalysts were dried under vacuum and used in new catalytic runs with a fresh set of reagents for cyanosilylation. Unfortunately, the corresponding product **2a** was obtained in 24 and 52% yields for **Y/Tb-MOF** and **Tb-MOF**, respectively (Figure S27), showing a loss of catalytic activity possibly due to an irreversible transformation of the MOF. The recyclability tests were also conducted under the same procedure for the hydroboration and CO_2 cycloaddition catalytic reactions, revealing distinct behaviors. While in the hydroboration reaction, the conversions decreased to 50% after the first cycle and further dropped to 34% after the second cycle (Figure 5), the conversions remained constant with no erosion throughout the four tested cycles in the cycloaddition process (Figure 5). The reason for the varying stability of the MOF catalyst in the three catalytic reactions could be attributed to the differing abilities of the Lewis acid metal centers to coordinate with the various substrates during
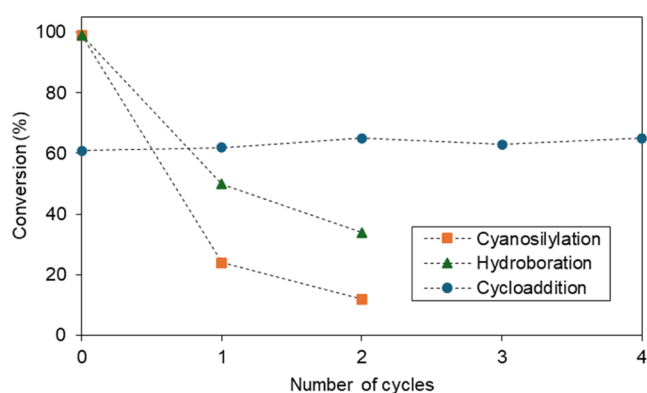

Figure 5. Study of the recyclability of the **Y/Tb-MOF** catalyst on the cyanosilylation (squares), hydroboration (triangles), and CO_2 cycloaddition (circles) reactions.

the reaction. However, further studies should be conducted to corroborate this statement. The PXRD diffractograms of the MOF before and after the fourth cycle are depicted in Figures S3 and S10. In the cycloaddition process, almost no variations in the diffraction patterns were observed, indicating minor transformations in the structural assembly during catalysis. These results align with the previously conducted gas adsorption experiments, where the anticipated interpenetration of the gas and higher loading capacity were observed. On the contrary, in the cyanosilylation and hydroboration reactions, the PXRD analysis of freshly prepared and recycled **Y/Tb-MOF** and **Tb-MOF** (Figures S2−S8) reveals a pattern change before and after the reaction. This further corroborates that under these conditions, the MOFs undergo alteration over time.

One of the most meaningful conclusions drawn from our studies is the recognition that the design of both monometallic and bimetallic MOFs, with this specific ligand, results in poor recyclability in the cyanosilylation and hydroboration reactions but not in the CO_2 cycloaddition of epoxides. This observation is not only relevant but also provides valuable insights into the limitations and challenges associated with the studied MOF systems.

To verify that the loss of catalytic activity in both cyanosilylation and hydroboration reactions was due to an irreversible transformation of the MOF and probable

Scheme 1. Leaching Test Carried Out Using Y/Tb-MOF as a Catalyst for (a) Cyanosilylation and (b) Hydroboration of 1a, 1d, and 1c
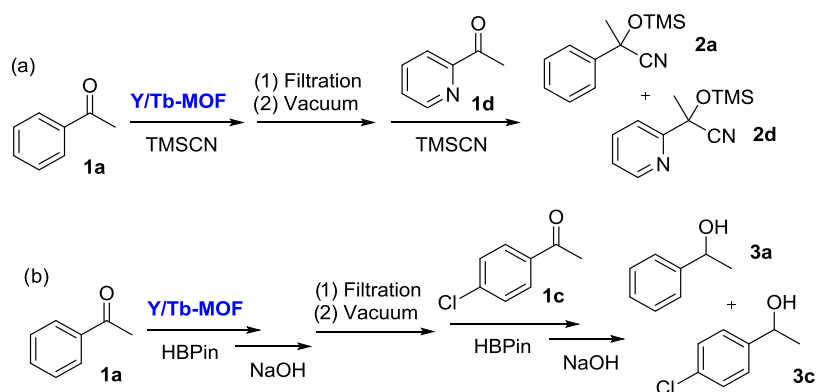
dissolution of some metal content in the reaction medium, leaching tests and ICP-MS analysis were conducted in the performance of the bimetallic Y/Tb catalyst. After the first reaction of the recyclability test, the supernatant obtained after the centrifugation was filtered through a plug of Celite, dried under vacuum, and used for ICP-MS analysis and catalysis. For the latter, in this dried filtrate, a different carbonylic substrate (1d or 1c) together with TMSCN (cyanosilylation) or HBpin (hydroboration) was added, and the reactions were conducted under the same optimal conditions (Scheme 1). After 24 h, an aliquot was analyzed using ^{1}H NMR, revealing 85 and 96% conversion rates in these subsequent reactions. The analysis indicated the presence of both products 2a/3a and 2d/3c in the reaction crudes, confirming the leaching of metals into the reaction media.

ICP-MS analysis revealed that in both catalyzed reactions, the leaching of metals, whether yttrium or terbium, occurred at equal concentrations, suggesting an equal leaching rate for both metals. This indicates that the erosion in catalytic activity observed across cycles is likely due to a transformation of the structure (confirmed by PXRD) and a reduction in metal loading in the solid state (confirmed with the catalytic experiments conducted with the filtrates). Interestingly, the ratio of leached metals remained nearly constant over the first two cycles, with Y/Tb ratios of 1.05 (2.21/2.10 μg/L) and 1.18 (4.08/3.46 μg/L) for the cyanosilylation reactions and 1.02 (2.75/2.69 μg/L) and 1.06 (2.47/2.33 μg/L) for the hydroboration reaction.

We also conducted a stability study of the catalysts under two conditions: (i) stirring in protic (water) and aprotic (chloroform) solvents and (ii) catalytic conditions. When both catalysts were stirred in water for 24 h at room temperature, UV spectra revealed peaks corresponding to the 3-amino-4-hydroxybenzoate ligand (see Figures S27–S29). Subsequent stirring of the resulting MOFs in water did not release any additional ligand into the solution, suggesting that some adsorbed free ligand remained in the channels of the MOFs after their synthesis, underscoring the importance of the workup steps. Stirring in chloroform did not result in any solubilization of the ligand, verifying the stability of the MOFs when stirred in both protic and aprotic solvents. When the MOF catalysts were allowed to react under solvent-free conditions in the presence of the corresponding reagents used in the three catalytic reactions studied (TMSCN, acetophenone, HBpin, and styrene oxide at 100 °C), no leaching of the benzoate ligand was detected. Interestingly,

only under CO_2 cycloaddition reaction conditions in the presence of the epoxide at 100 °C was DMF observed in the filtrate, thus being the sole delivered compound. These results suggest that under catalytic conditions, the MOFs remain stable, but it is during substrate catalytic transformation that they become gradually inactivated.

Green Chemistry Metrics. In order to evaluate if the overall transformations were eco-friendly and overcome health and environmental problems derived from the chemical industry,[52,53] green chemistry metrics such as atomic economy (AE), mass intensity (MI), reaction mass efficiency (RME), and carbon efficiency (CE) were calculated as previously described by Gomez et al.[18,39] and by us.[19,21,34,35] Table S9 shows the green chemistry metrics for the catalytic reactions studied. The AE (100%), MI (1.1), RME (94.7%), and CE (95.8%) values for Y/Tb-MOF and Tb-MOF catalysts in the cyanosilylation reaction for acetophenone (1a) are comparable to those described previously for related lanthanide-based MOFs.[18,34,35,39,44] The values obtained for the hydroboration reaction using acetophenone (1a) as the starting material with Y/Tb-MOF were 49.2% for AE, 2.4 for MI, 42.6% for RME, and 49.9% for CE, and with the Tb-MOF catalyst, the values were 49.2% for AE, 3.2 for MI, 32.8% for RME, and 38.4% for CE. Table S10 provides all metric values for all of the assayed carbonyls. These values decreased considerably when compared to the cyanosilylation reaction due to the large loss of atoms of the final product as a consequence of the hydrolysis of the borate intermediate, being similar to those obtained previously.[35] In the cycloaddition reaction, the green metrics are similar to those obtained in the cyanosilylation reaction in terms of AE with 100% in substrates 4a–c, better regarding MI with values of 4.1–8.3%, and significantly reduced in terms of RME and CE with values in the range of 12.8–27.3% and 20.3–43.0%, respectively (Table S11).

Materials and Methods. All experiments involving moisture-sensitive compounds were performed under an inert atmosphere of N_2 using standard techniques. Unless otherwise indicated, reagents and substrates were purchased from commercial sources and used as received. Metallic precursors, such as terbium(III) nitrate pentahydrate (99.9%, Alfa Aesar) and yttrium(III) nitrate hexahydrate (99.9% of purity, Fluorochem), were used as received, as well as the 3-amino-4-hydroxybenzoic acid ligand (H$_2$L, C$_7$H$_7$NO$_3$, 97% of purity), which was purchased from Fluorochem. Solvents not required to be dry were purchased as technical grade and used as received. Conversion values relative to the limiting reagent

were calculated from the ^1H NMR spectra of the reaction crudes. For further details regarding the general procedures and analytical methods used, see the Supporting Information.

CONCLUSIONS

In summary, we have synthesized and characterized a new heterobimetallic MOF (**Y/Tb-MOF**) with a 3.5:1.5 yttrium/terbium composition. This novel material underwent comprehensive characterization through PXRD, SCXRD, FTIR, SEM-EDX, and ICP-MS analyses. The resulting bimetallic MOF demonstrates isostructural properties similar to those of some previously described monometallic MOFs based on Dy, Y, Eu, and Tb and another bimetallic MOF of Y/Eu, with minor alterations in structural assemblies, resulting in a cell volume change of less than 3%.

The newly developed bimetallic Y/Tb system, along with the monometallic isostructural congener of Tb, was applied in the solvent-free cyanosilylation and hydroboration of ketones, facilitating green transformations under ambient conditions and with reduced catalyst loadings of 0.5 mol %, albeit with poor recyclability. Conversely, the heterobimetallic MOF exhibited promising performance in the cycloaddition of epoxides and carbon dioxide, achieving conversions in the range of 46−87% and demonstrating recyclability for up to four cycles without erosion of catalytic performance.

Our ongoing work in ligand design aims to identify synergistic metal combinations within the catalyst framework and explore the asymmetric variants of these reactions.

ASSOCIATED CONTENT

⒮ⓘ Supporting Information

The Supporting Information is available free of charge at https://pubs.acs.org/doi/10.1021/acsomega.4c03109.

> General experimental information; general procedures; crystallographic data; selected bond lengths and angles data; experimental PXRD, FTIR analysis of the ligand and catalyst; particle size distribution of catalysts; study of ζ-potential at different pH values and size distribution; TOF and TON data; characterization data of products; NMR data; leaching test; UV−vis measurements; green chemistry metrics; recyclability of the catalysts; and bibliographic reviews on previous results obtained with to-date-reported RE-based MOF catalysts (PDF)

AUTHOR INFORMATION

Corresponding Authors

Iñigo J. Vitorica-Yrezabal − *Department of Inorganic Chemistry, University of Granada, 18071 Granada, Spain;* ⓞ orcid.org/0000-0001-8806-150X; Email: vitorica@ugr.es

Ignacio Fernández − *Department of Chemistry and Physics, Research Centre CIAIMBITAL, University of Almería, 04120 Almería, Spain;* ⓞ orcid.org/0000-0001-8355-580X; Email: ifernan@ual.es

Authors

Mireya E. López-Vargas − *Department of Chemistry and Physics, Research Centre CIAIMBITAL, University of Almería, 04120 Almería, Spain;* ⓞ orcid.org/0000-0001-8200-2824

Juana M. Pérez − *Department of Chemistry and Physics, Research Centre CIAIMBITAL, University of Almería, 04120 Almería, Spain;* ⓞ orcid.org/0000-0002-6495-2591

Estitxu Echenique-Errandonea − *Departamento de Química Aplicada, Universidad del País Vasco UPV/EHU, 20018 Donostia-San Sebastián, Spain*

Arantxa Forte-Castro − *Department of Chemistry and Physics, Research Centre CIAIMBITAL, University of Almería, 04120 Almería, Spain*

Sara Rojas − *Department of Inorganic Chemistry, University of Granada, 18071 Granada, Spain;* ⓞ orcid.org/0000-0002-7874-2122

José M. Seco − *Departamento de Química Aplicada, Universidad del País Vasco UPV/EHU, 20018 Donostia-San Sebastián, Spain*

Antonio Rodríguez-Diéguez − *Department of Inorganic Chemistry, University of Granada, 18071 Granada, Spain;* ⓞ orcid.org/0000-0003-3198-5378

Complete contact information is available at:
https://pubs.acs.org/10.1021/acsomega.4c03109

Author Contributions

The manuscript was written through contributions of all authors. All authors have given approval to the final version of the manuscript.

Notes

The authors declare no competing financial interest.

ACKNOWLEDGMENTS

REFERENCES

(1) Rao, R.; Ma, S.; Gao, B.; Bi, F.; Chen, Y.; Yang, Y.; Liu, N.; Wu, M.; Zhang, X. Recent Advances of Metal-Organic Framework-Based and Derivative Materials in the Heterogeneous Catalytic Removal of Volatile Organic Compounds. *J. Colloid Interface Sci.* **2023**, *636*, 55−72.

(2) Remya, V. R.; Kurian, M. Synthesis and Catalytic Applications of Metal−Organic Frameworks: A Review on Recent Literature. *Int. Nano Lett.* **2019**, *9* (1), 17−29.

(3) Zhou, H. C. J.; Kitagawa, S. Metal-Organic Frameworks (MOFs). *Chem. Soc. Rev.* **2014**, *43* (16), 5415−5418.

(4) Chen, L.; Zhang, X.; Cheng, X.; Xie, Z.; Kuang, Q.; Zheng, L. The Function of Metal-Organic Frameworks in the Application of MOF-Based Composites. *Nanoscale Adv.* **2020**, *2* (7), 2628−2647.

(5) Pascanu, V.; Miera, G. G.; Inge, A. K.; Martín-Matute, B. Metal-Organic Frameworks as Catalysts for Organic Synthesis: A Critical Perspective. *J. Am. Chem. Soc.* **2019**, *141* (18), 7223−7234.

(6) Le, D. H.; Loughan, R. P.; Gładysiak, A.; Rampal, N.; Brooks, I. A.; Park, A. H. A.; Fairen-Jimenez, D.; Stylianou, K. C. Lanthanide Metal−Organic Frameworks for the Fixation of CO_2 under Aqueous-Rich and Mixed-Gas Conditions. *J. Mater. Chem. A* **2022**, *10* (3), 1442−1450.

(7) Tan, K. X.; Li, K.; Zheng, Z. J.; Lin, X. L.; Liu, Y. F.; Zhang, Z. B.; Yang, G. P. Two-Fold Interpenetrated Binuclear Nickel Metal-Organic Framework as a Heterogeneous Catalyst for N-Heterocycle Synthesis. *Inorg. Chem.* 2023, 62, 17310−17316.

(8) Liu, Y. F.; Lin, X. L.; Ming, B. M.; Hu, Q. L.; Liu, H. Q.; Chen, X. J.; Liu, Y. H.; Yang, G. P. Three Polyoxometalate-Based Ag-Organic Compounds as Heterogeneous Catalysts for the Synthesis of Benzimidazoles. *Inorg. Chem.* 2024, 63, 5681−5688.

(9) Cabrero-Antonino, M.; Remiro-Buenamañaña, S.; Souto, M.; Garciá-Valdivia, A. A.; Choquesillo-Lazarte, D.; Navalón, S.; Rodríguez-Diéguez, A.; Espallargas, G. M.; Garciá, H. Design of Cost-Efficient and Photocatalytically Active Zn-Based MOFs Decorated with Cu₂O Nanoparticles for CO₂ Methanation. *Chem. Commun.* 2019, 55 (73), 10932−10935, DOI: 10.1039/C9CC04446A.

(10) Lee, J.; Farha, O. K.; Roberts, J.; Scheidt, K. A.; Nguyen, S. T.; Hupp, J. T. Metal-Organic Framework Materials as Catalysts. *Chem. Soc. Rev.* 2009, 38 (5), 1450−1459.

(11) Chen, L.; Wang, H. F.; Li, C.; Xu, Q. Bimetallic Metal-Organic Frameworks and Their Derivatives. *Chem. Sci.* 2020, 11 (21), 5369−5403.

(12) Dhakshinamoorthy, A.; Asiri, A. M.; Garcia, H. Mixed-Metal or Mixed-Linker Metal Organic Frameworks as Heterogeneous Catalysts. *Catal. Sci. Technol.* 2016, 6 (14), 5238−5261.

(13) Abednatanzi, S.; Derakhshandeh, P. G.; Depauw, H.; Coudert, F. X.; Vrielinck, H.; Van Der Voort, P.; Leus, K. Mixed-Metal Metal-Organic Frameworks. *Chem. Soc. Rev.* 2019, 48 (9), 2535−2565.

(14) He, H.; Perman, J. A.; Zhu, G.; Ma, S. Metal-Organic Frameworks for CO₂ Chemical Transformations. *Small* 2016, 12 (46), 6309−6324.

(15) Chen, H.; Liu, S.; Lv, H.; Qin, Q. P.; Zhang, X. Nanoporous {Y2}-Organic Frameworks for Excellent Catalytic Performance on the Cycloaddition Reaction of Epoxides with CO₂ and Deacetalization-Knoevenagel Condensation. *ACS Appl. Mater. Interfaces* 2022, 14 (16), 18589−18599.

(16) Wei, N.; Zuo, R. X.; Zhang, Y. Y.; Han, Z. B.; Gu, X. J. Robust High-Connected Rare-Earth MOFs as Efficient Heterogeneous Catalysts for CO₂ Conversion. *Chem. Commun.* 2017, 53 (22), 3224−3227.

(17) Wu, P.; Wang, J.; Li, Y.; He, C.; Xie, Z.; Duan, C. Luminescent Sensing and Catalytic Performances of a Multifunctional Lanthanide-Organic Framework Comprising a Triphenylamine Moiety. *Adv. Funct. Mater.* 2011, 21 (14), 2788−2794.

(18) Gomez, G. E.; Kaczmarek, A. M.; Van Deun, R.; Brusau, E. V.; Narda, G. E.; Vega, D.; Iglesias, M.; Gutierrez-Puebla, E.; Monge, M. Á. Photoluminescence, Unconventional-Range Temperature Sensing, and Efficient Catalytic Activities of Lanthanide Metal-Organic Frameworks. *Eur. J. Inorg. Chem.* 2016, 2016 (10), 1577−1588.

(19) Pérez, J. M.; Rojas, S.; García-García, A.; Montes-Andrés, H.; Martínez, C. R.; Romero-Cano, M. S.; Choquesillo-Lazarte, D.; Abdelkader-Fernández, V. K.; Pérez-Mendoza, M.; Cepeda, J.; Rodríguez-Diéguez, A.; Fernández, I. Catalytic Performance and Electrophoretic Behavior of an Yttrium-Organic Framework Based on a Tricarboxylic Asymmetric Alkyne. *Inorg. Chem.* 2022, 61 (3), 1377−1384.

(20) Pagis, C.; Ferbinteanu, M.; Rothenberg, G.; Tanase, S. Lanthanide-Based Metal Organic Frameworks: Synthetic Strategies and Catalytic Applications. *ACS Catal.* 2016, 6 (9), 6063−6072.

(21) Pérez, J. M.; Echenique-Errandonea, E.; Rojas, S.; Choquesillo-Lazarte, D.; Seco, J. M.; López-Vargas, M. E.; Rodríguez-Diéguez, A.; Fernández, I. Improved Performance of a Europium-Based Metal-Organic Framework for Cyanosilylation of Demanding Ketones. *ChemCatChem* 2022, 14, No. e2022009.

(22) Kajiwara, T.; Higuchi, M.; Yuasa, A.; Higashimura, H.; Kitagawa, S. One-Dimensional Alignment of Strong Lewis Acid Sites in a Porous Coordination Polymer. *Chem. Commun.* 2013, 49 (89), 10459−10461.

(23) Dvries, R. F.; De La Peña-Oshea, V. A.; Snejko, N.; Iglesias, M.; Gutiérrez-Puebla, E.; Monge, M. Á. Insight into the Correlation between Net Topology and Ligand Coordination Mode in New Lanthanide MOFs Heterogeneous Catalysts: A Theoretical and Experimental Approach. *Cryst. Growth Des.* 2012, 12 (11), 5535−5545.

(24) Dvries, R. F.; Snejko, N.; Iglesias, M.; Gutiérrez-Puebla, E.; Monge, M. A. Ln-MOF Pseudo-Merohedral Twinned Crystalline Family as Solvent-Free Heterogeneous Catalysts. *Cryst. Growth Des.* 2014, 14 (5), 2516−2521.

(25) Batista, P. K.; Alves, D. J. M.; Rodrigues, M. O.; De Sá, G. F.; Junior, S. A.; Vale, J. A. Tuning the Catalytic Activity of Lanthanide-Organic Framework for the Cyanosilylation of Aldehydes. *J. Mol. Catal. A* 2013, 379, 68−71.

(26) An, H.; Wang, L.; Hu, Y.; Fei, F. Temperature-Induced Racemic Compounds and Chiral Conglomerates Based on Poly-oxometalates and Lanthanides: Syntheses, Structures and Catalytic Properties. *CrystEngComm* 2015, 17 (7), 1531−1540.

(27) Fei, F.; An, H.; Meng, C.; Wang, L.; Wang, H. Lanthanide-Supported Molybdenum-Vanadium Oxide Clusters: Syntheses, Structures and Catalytic Properties. *RSC Adv.* 2015, 5 (24), 18796−18805.

(28) Wang, X.; Zhang, L.; Yang, J.; Liu, F.; Dai, F.; Wang, R.; Sun, D. Lanthanide Metal − Organic Frameworks Containing a Novel Fl Exible Ligand for Luminescence Sensing of Small Organic Molecules and Selective Adsorption. *J. Mater. Chem. A* 2015, 00, 1−9.

(29) Zhu, C.; Xia, Q.; Chen, X.; Liu, Y.; Du, X.; Cui, Y. Chiral Metal − Organic Framework as a Platform for Cooperative Catalysis in Asymmetric Cyanosilylation of Aldehydes. *ACS Catal.* 2016, 6, 7590−7596, DOI: 10.1021/acscatal.6b02359.

(30) Liu, X.; Lin, H.; Xiao, Z.; Fan, W.; Huang, A.; Wang, R.; Zhang, L.; Sun, D. Multifunctional Lanthanide-Organic Frameworks for Fluorescent Sensing, Gas Separation and Catalysis. *Dalton Trans.* 2016, 45 (9), 3743−3749.

(31) Gustafsson, M.; Bartoszewicz, A.; Martiín-Matute, B.; Sun, J.; Grins, J.; Zhao, T.; Li, Z.; Zhu, G.; Zou, X. A Family of Highly Stable Lanthanide Metal-Organic Frameworks: Structural Evolution and Catalytic Activity. *Chem. Mater.* 2010, 22 (11), 3316−3322.

(32) Zhu, Y.; Zhu, M.; Xia, L.; Wu, Y.; Hua, H.; Xie, J. Lanthanide Metal-Organic Frameworks with Six-Coordinated Ln(III) Ions and Free Functional Organic Sites for Adsorptions and Extensive Catalytic Activities. *Sci. Rep.* 2016, 6 (April), 1−11.

(33) Zhu, Y.; Wang, Y.; Liu, P.; Xia, C.; Wu, Y.; Lu, X.; Xie, J. Two Chelating-Amino-Functionalized Lanthanide Metal-Organic Frameworks for Adsorption and Catalysis. *Dalton Trans.* 2015, 44 (4), 1955−1961.

(34) Echenique-Errandonea, E.; Pérez, J. M.; Rojas, S.; Cepeda, J.; Seco, J. M.; Fernández, I.; Rodríguez-Diéguez, A. A Novel Yttrium-Based Metal-Organic Framework for the Efficient Solvent-Free Catalytic Synthesis of Cyanohydrin Silyl Ethers. *Dalton Trans.* 2021, 50 (34), 11720−11724.

(35) Echenique-Errandonea, E.; López-Vargas, M. E.; Pérez, J. M.; Rojas, S.; Choquesillo-Lazarte, D.; Seco, J. M.; Fernández, I.; Rodríguez-Diéguez, A. A Mixed Heterobimetallic Y/Eu-MOF for the Cyanosilylation and Hydroboration of Carbonyls. *Catalysts* 2022, 12 (3), 299.

(36) Pérez, J. M.; Morales-Cámara, S.; García-Salas, F. M.; Ruiz-Cuevas, N.; López-Vargas, M. E.; Choquesillo-Lazarte, D.; Cepeda, J.; García, J. A.; Abdelkader-Fernández, V. K.; Rodríguez-Diéguez, A.; Rojas, S.; Fernández, I. Metal−Organic Frameworks Based on a Janus-Head Biquinoline Ligand as Catalysts in the Transformation of Carbonyl Compounds into Cyanohydrins and Alcohols. *Cryst. Growth Des.* 2022, 22, 7395.

(37) Karmakar, A.; Rúbio, G. M. D. M.; Paul, A.; da Silva, M. F. C. G.; Mahmudov, K. T.; Guseinov, F. I.; Carabineiro, S. A. C.; Pombeiro, A. J. L. Lanthanide Metal Organic Frameworks Based on Dicarboxyl-Functionalized Arylhydrazone of Barbituric Acid: Syntheses, Structures, Luminescence and Catalytic Cyanosilylation of Aldehydes. *Dalton Trans.* 2017, 46 (26), 8649−8657, DOI: 10.1039/C7DT01056G.

(38) He, H.; Ma, H.; Sun, D.; Zhang, L.; Wang, R.; Sun, D. Porous Lanthanide-Organic Frameworks: Control over Interpenetration, Gas Adsorption, and Catalyst Properties. *Cryst. Growth Des.* **2013**, *13* (7), 3154−3161.

(39) Gomez, G. E.; Brusau, E. V.; Sacanell, J.; Soler Illia, G. J. A. A.; Narda, G. E. Insight into the Metal Content-Structure-Property Relationship in Lanthanide Metal-Organic Frameworks: Optical Studies, Magnetism, and Catalytic Performance. *Eur. J. Inorg. Chem.* **2018**, *2018* (20−21), 2452−2460.

(40) Wu, X.; Lin, Z.; He, C.; Duan, C. Catalytic Performance of Lanthanide Molecular Solids Containing Well-Modified Metal-Organic Octahedra. *New J. Chem.* **2012**, *36* (1), 161−167.

(41) Wu, P.; Xia, L.; Huangfu, M.; Fu, F.; Wang, M.; Wen, B.; Yang, Z.; Wang, J. Lanthanide-Based Metal-Organic Frameworks Containing "v-Shaped" Tetracarboxylate Ligands: Synthesis, Crystal Structures, "Naked-Eye" Luminescent Detection, and Catalytic Properties. *Inorg. Chem.* **2020**, *59* (1), 264−273.

(42) Evans, O. R.; Ngo, H. L.; Lin, W. Chiral Porous Solids Based on Lamellar Lanthanide Phosphonates. *J. Am. Chem. Soc.* **2001**, *123* (42), 10395−10396.

(43) Dvries, R. F.; Iglesias, M.; Snejko, N.; Gutiérrez-Puebla, E.; Monge, M. A. Lanthanide Metal-Organic Frameworks: Searching for Efficient Solvent-Free Catalysts. *Inorg. Chem.* **2012**, *51* (21), 11349−11355.

(44) Echenique-Errandonea, E.; Mendes, R. F.; Figueira, F.; Choquesillo-Lazarte, D.; Beobide, G.; Cepeda, J.; Ananias, D.; Rodríguez-Diéguez, A.; Paz, F. A. A.; Seco, J. M. Multifunctional Lanthanide-Based Metal-Organic Frameworks Derived from 3-Amino-4-Hydroxybenzoate: Single-Molecule Magnet Behavior, Luminescent Properties for Thermometry, and CO2 Adsorptive Capacity. *Inorg. Chem.* **2022**, *61* (33), 12977−12990, DOI: 10.1021/acs.inorgchem.2c00544.

(45) Prakash, A.; Saini, S.; Basappa, S.; Gupta, D. K.; Mao, L.; Bose, S. K. Metal-Organic Frameworks for Catalytic Construction of C−B Bond and Related Reactions. *ChemCatChem* **2023**, *15* (1), No. e202201156, DOI: 10.1002/cctc.202201156.

(46) Magre, M.; Szewczyk, M.; Rueping, M. S-Block Metal Catalysts for the Hydroboration of Unsaturated Bonds. *Chem. Rev.* **2022**, *122*, 8261.

(47) Sun, X.; Gong, X.; Xie, Z.; Zhu, C. A Uranium(IV) Alkyl Complex: Synthesis and Catalytic Property in Carbonyl Hydroboration. *Chin. J. Chem.* **2022**, *40* (17), 2047−2053.

(48) Link, L.; Niewa, R. Polynator : A Tool to Identify and Quantitatively Evaluate Polyhedra and Other Shapes in Crystal Structures. *J. Appl. Crystallogr.* **2023**, *56* (6), 1855−1864.

(49) Spek, A. L. Structure Validation in Chemical Crystallography. *Acta Crystallogr., Sect. D: Biol. Crystallogr.* **2009**, *65* (2), 148−155.

(50) Shannon, R. D. Revised Effective Ionic Radii and Systematic Studies of Interatomie Distances in Halides and Chaleogenides. *Acta Crystallogr.* **1976**, *A32*, 751−767.

(51) Dong, J.; Cui, P.; Shi, P. F.; Cheng, P.; Zhao, B. Ultrastrong Alkali-Resisting Lanthanide-Zeolites Assembled by [Ln60] Nanocages. *J. Am. Chem. Soc.* **2015**, *137* (51), 15988−15991.

(52) Constable, D. J. C.; Curzons, D.; Cunningham, V. L. Metrics to 'green' chemistry—which are the best? *Green Chem.* **2002**, *4*, 521−527, DOI: 10.1039/B206169B.

(53) Trost, B. M. The Atom Economy - A Search for Synthetic Efficiency. *Science* **1991**, *254* (5032), 1471−1477, DOI: 10.1126/science.1962206.